# Finite-size scaling study of the vapor-liquid critical properties of confined fluids: Crossover from three dimensions to two dimensions

Yang Liu, Athanassios Z. Panagiotopoulos, and Pablo G. Debenedetti[a)]
*Department of Chemical Engineering, Princeton University, Princeton, New Jersey 08544, USA*

(Received 12 February 2010; accepted 11 March 2010; published online 8 April 2010)

We perform histogram-reweighting grand canonical Monte Carlo simulations of the Lennard-Jones fluid confined between two parallel hard walls and determine the vapor-liquid critical and coexistence properties in the range of $\sigma \leq H \leq 6\sigma$ and $10\sigma \leq L_x, L_y \leq 28\sigma$, where $H$ is the wall separation, $L_x = L_y$ is the system size and $\sigma$ is the characteristic length. By matching the probability distribution of the ordering operator, $P(M)$, to the three-dimensional (3D) and two-dimensional (2D) Ising universality classes according to the mixed-field finite-size scaling approach, we establish a "phase diagram" in the $(H,L)$ plane, showing the boundary between four types of behavior: 3D, quasi-3D, quasi-2D, and 2D. In order to facilitate 2D critical point calculation, we present a four-parameter analytical expression for the 2D Ising universal distribution. We show that the infinite-system-size critical points obtained by extrapolation from the apparent 3D and 2D critical points have only minor differences with each other. In agreement with recent reports in the literature [Jana *et al.*, J. Chem. Phys. **130**, 214707 (2009)], we find departure from linearity in the relationship between critical temperature and inverse wall separation, as well as nonmonotonic dependence of the critical density and the liquid density at coexistence upon wall separation. Additional studies of the ST2 model of water show similar behavior, which suggests that these are quite general properties of confined fluids. © *2010 American Institute of Physics*. [doi:10.1063/1.3377089]

## I. INTRODUCTION

Confined fluids are commonly encountered in biology, geology, and industry. Knowledge of the phase behavior and thermodynamic properties of fluids in confinement is essential for understanding natural phenomena such as membrane mechanics,[1] capillary condensation,[2] and protein folding;[3] for the engineering design of industrial processes, such as oil recovery and heterogeneous catalysis; and for implementing technological solutions to address environmental problems.[4] An example of the latter category is knowledge of the phase behavior in $CO_2$-water systems under conditions relevant to carbon capture and storage, and how it is affected by nanoscale confinement, such as could occur during flow in narrow pores during a leak.[5]

The phase behavior of fluids can be greatly affected by the presence of solid surfaces. It is customary to distinguish interfacial effects, which arise when a fluid contacts a solid surface from confinement effects, which occur when a fluid system is surrounded by solid boundaries, and the characteristic confining dimension is comparable to the size of a molecule. Examples of the former include the occurrence of surface transitions which are absent in the bulk, such as layering and wetting.[2,6,7] Examples of the latter include the shift in the common phase transitions, such as the vapor-liquid transition[8–13] and the liquid-liquid transition for binary mixtures.[14–16] The effects of confinement on the phase behavior of fluids, if properly understood, can be used as a powerful tool to probe the thermodynamic properties of the confined fluid. A recent important application of confinement in scientific research is the suppression of ice nucleation and the consequent ability to study deeply supercooled water below its homogenous nucleation temperature by confinement in nanosize pores.[17–27] Evidence of a fragile-to-strong dynamic transition in confined supercooled water has been obtained,[19–23,27] yet its relation to bulk phase behavior, in particular the proposed liquid-liquid transition of supercooled water,[28] remains controversial due to conflicting interpretations of the effects of confinement on experimental measurements,[20,29,30] and more generally the lack of a sound theoretical basis with which to relate measurements on a confined system to the thermodynamics of the corresponding bulk system.

Recently we used histogram reweighting grand canonical Monte Carlo (GCMC)[31,32] and mixed-field finite-size scaling[33,34] to locate the liquid-liquid critical point of the ST2 model of water[35] at $T_c = 237 \pm 4$ K, $\rho_c = 0.99 \pm 0.02$ g/cc, and $P_c = 167 \pm 24$ MPa.[36] It is desirable to implement this rigorous method to confined water systems, since understanding to what extent various types of confinement (e.g., hydrophobic and hydrophilic) shift this critical point and affect this transition will provide valuable quantitative predictions that bridge experiments and computations. At present, however, the application of the mixed-field finite-size scaling approach to confined systems is not straightforward. The premise for applying finite-size scaling is that the phase transition belongs to the Ising universality class.[33,34] Depending on the dimensionality of the system, either the three-dimensional (3D) (Ref. 34) or the two-dimensional (2D) universality class[37] should apply at the infinite system size limit.

[a)]Author to whom correspondence should be addressed. Electronic mail: pdebene@princeton.edu.

 

In confinement, however, the introduction of geometric constraints complicates the determination of the effective dimensionality of the system at finite system sizes, and therefore complicates the accurate determination of critical points.

The effect of dimensionality on the critical behavior of confined systems has been the subject of extensive theoretical investigations spanning several decades,[2,6,38–44] and a dimensional crossover from the 3D to the 2D universality class (in terms of critical exponents,[45] and based on the general finite-size scaling theory[46,47]) has been observed in many systems, such as Ising models,[40,43] soft matter mixtures,[48–50] square-well fluids,[11,12] and water.[51] In very narrow pores, 2D critical behavior is expected[2] and has been confirmed in experiments[52] and simulations.[11,43,49,53,54] However, for large enough pores, such that most fluid molecules do not "feel" the surfaces, 3D critical behavior is approached[6,51]even quite near the critical point. The observed effective critical exponents are found to be sensitive to system size as well.[12] While the above studies mainly focused on smooth, or on regular, atomically detailed walls, it is found that in random confinement, such as for example gels, the critical behavior belongs instead to the random-field Ising universality class.[55,56] The only previous work to our knowledge that applied the mixed-field finite-size scaling approach of Wilding[33,34] to confined systems is the study of the phase transitions of confined lattice homopolymers,[54] where large system sizes were used and the critical parameters were determined by matching the probability distribution of the ordering operator of the system, which is a combination of the number of particles and the energy, to the 2D universality class. However, it is not always the case that the 2D limit can be approached, due to the increasing computational effort required for larger pore widths. Here we focus our attention on continuous-space models, and we investigate the extent to which matches to the 2D universality class are possible for system sizes that can be explored in practical simulations. More specifically, we explore the existence and location of the 3D to 2D crossover as a function of pore width and system size, based on the probability distribution of the order operator of the system.

To tackle the problem, we consider the vapor-liquid transition of the Lennard-Jones (LJ) fluid confined by hard walls. The LJ potential is a basic model that has been extensively used to represent monoatomic fluids.[57] It is also frequently used as part of the force field in simulating molecular fluids, such as water,[35] methanol,[58] and carbon dioxide.[59] The vapor-liquid coexistence properties of both the bulk[34,60,61] and 2D LJ fluids[53,61] have been investigated comprehensively. Using histogram reweighting GCMC and the mixed-field finite-size scaling approach, we examine the matches of the probability distribution of the ordering operator of the system to the 2D and 3D universality class distributions, and locate the effective critical points at various wall separations and simulation box sizes. The effects of confinement on the critical parameters and coexistence densities are also of considerable scientific interest. One important conclusion from previous theoretical predictions[2,6] and computer simulations[62] is the existence of a linear relationship between the shift in the critical temperature and inverse wall separation in narrow pores. Recently, however, this linear dependence was found to break down in extremely narrow pores (one or two fluid layers) in studies of the vapor-liquid transition of the square-well fluid confined by hard walls,[11,12] as well as the vapor-liquid transition of alkanes in graphite and mica pores.[13] Remarkably, the critical density was found to decrease as the pore width increased initially from the strictly 2D case, but then increased until it reached a maximum at a separation corresponding to two layers of fluid molecules within the pore.[12] The calculations reported here for the vapor-liquid transition of the confined LJ fluid, as well as for the confined ST2 model of water, the latter being representative of fluids with short-range directional and long-range electrostatic interactions, reveal similar behavior for the evolution of the critical temperature, critical density, and the coexisting densities to that found in the square-well fluid.[11,12] This suggests that the departure from linearity in the relationship between critical temperature and inverse pore width, as well as the nonmonotonic dependence of the critical density upon pore width, are quite general properties of confined fluids.

As an additional result of this work, we provide a simple, four-parameter analytical expression for the 2D Ising universal distribution. The 2D and 3D Ising universal distributions are extensively used in finite-size scaling studies. The Ising universal distributions have been obtained from numerical simulations: for example, Hilfer and Wilding[63] provided accurate determinations of the 2D and 3D Ising universal distributions by extensive MC simulations. In 2000, Tsypin and Blöte formulated a highly accurate two-parameter analytical expression for the 3D Ising universal distribution.[64] Inspired by this work, as well as other theoretical and computational studies,[63,65] we propose an analytical expression for the 2D Ising universal distribution which we find to be of satisfactory accuracy and convenient for future use. The details of this expression are provided in the Appendix.

This paper is organized as follows. Model system and simulation details are provided in Sec. II. Results and discussion are presented in Sec. III. The major conclusions of this work are presented in Sec. IV, followed by an Appendix.

## II. MODEL SYSTEM AND SIMULATION DETAILS

In this study, the LJ fluid is confined between two parallel structureless hard walls. Periodic boundary conditions are applied in the $x$ and $y$ directions and the system is finite in the $z$ direction. The LJ potential is given by

$$\phi(r) = 4\varepsilon\left[\left(\frac{\sigma}{r}\right)^{12} - \left(\frac{\sigma}{r}\right)^{6}\right], \tag{1}$$

where $\phi$ is the pair potential, $\varepsilon$ and $\sigma$ are the characteristic energy and size parameters, respectively, and $r$ is the distance between two particles. Here, the LJ potential is truncated at $r_c = 2.5\sigma$ and no long-range corrections are included. Potential truncation has a measurable effect on the phase behavior and critical parameters.[66] The interaction between fluid particles and the hard walls is given by

$$\phi_{f\text{-}w} = \begin{cases} \infty, & r_{f\text{-}w} < \sigma \\ 0, & \sigma \le r_{f\text{-}w}, \end{cases} \tag{2}$$

where $r_{f\text{-}w}$ is the distance between the fluid particle and the wall in the $z$ direction. The simulation box lengths are set to be equal in the $x$ and $y$ directions, $L_x = L_y$, and they cover the range of $10\sigma \le L_x, L_y \le 28\sigma$. The range of wall separations $H$ studied in this work is $\sigma \le H \le 6\sigma$.

The dimensionless temperature is defined as $T^* = k_B T/\varepsilon$, where $k_B$ is Boltzmann's constant, and the dimensionless chemical potential is given by

$$\mu^* = \frac{1}{\varepsilon}(\mu^{ex} + k_B T \ln \rho\sigma^3) = \frac{1}{\varepsilon}\left(\mu + k_B T \ln \frac{\sigma^3}{\Lambda^3}\right), \tag{3}$$

where $\Lambda$ is the thermal de Broglie wavelength, and $\mu^{ex}$ is the difference between the chemical potential and that of an ideal gas at the same temperature and density. The density of the system is defined by $\rho^* = N\sigma^3/V$, with $N$ being the total number of particles and $V$ $(=L_x L_y H)$ being the total volume of the confined system. We take $H$ to be the distance between the two parallel hard repulsive walls. This definition of confined volume has been shown to be preferable to the alternative $\rho^* = N\sigma^3/V_h$ in comparing thermodynamic quantities of confined and bulk fluids, where $V_h$ $[=L_x L_y(H\text{-}\sigma)]$ is the volume accessible to particle centers.[67]

GCMC simulations were performed at fixed volume $V$, temperature $T$ and chemical potential $\mu$. The simulations started with an empty box and microstates were generated with a combination of displacement, insertion and deletion moves. To accept or reject moves, Metropolis criteria[68] were adopted. The maximum displacement of particles was $0.3\sigma$. At each step, the ratio of the probabilities of attempting displacement, insertion and deletion moves was 1:5:5. Throughout the simulations, the acceptance ratio was roughly 30%–50% for displacement moves, and 20%–40% for insertion/deletion moves. 2D histograms in the space of $N$ and $U$ were collected with an energy bin of $2\varepsilon$ after equilibration. The total number of MC steps used to produce the histograms ranged from 100 to $1000 \times 10^6$ steps, depending on the thermodynamic conditions and the box size. The longest simulations in a box of $L_x = L_y = 22\sigma$ and $H = 6\sigma$ took approximately 12 h on 3 GHz Xeon processors.

For each simulation box, that is, each wall separation $H$ and box length $L_x$ and $L_y$, the probability distribution of the density near the vapor-liquid critical point was first determined using histogram reweighting techniques.[31,32] Specifically, multiple runs covering a broad range of density and energy were conducted, and histograms were combined and reweighted to conditions of interest until a bimodal distribution of densities was found, which indicated the existence of a phase transition. New runs were then conducted at these specific conditions ($T$ and $\mu$) for sufficient MC steps to collect histogram data. The histogram data near the critical point were then used for precise determination of the critical point.

The mixed-field finite-size scaling theory of Wilding *et al.*[33,34] has been widely applied to determine critical parameters of 3D,[34,60,69,70,36,71] 2D,[37,72] and confined systems.[54] This approach defines an ordering operator $M$, which is a linear combination of the number of particles $N$ and total configurational energy $U$

$$M = N - sU, \tag{4}$$

where $s$ is the field mixing parameter. At criticality, the probability distribution of the scaling parameter of $x$, which is defined as $x = A(M - M_c)$, has a universal form. Depending on the dimensionality of the system, the vapor-liquid transition belongs to the 2D or the 3D universality class of the Ising model. Accordingly, the distribution can have one of two limiting forms: the 2D universal distribution[63,65] or the 3D universal distribution.[63,64] The nonuniversal parameter $A$ and the critical value of the ordering operator $M_c$ are chosen so that zero mean and unit variance of the distribution are observed in the scaling parameter. To obtain the critical parameters, we adjusted the thermodynamic parameters $T$, $\mu$ and the field mixing parameter $s$ to get a best fit to the universal distributions. The objective function used to minimize the deviation of the probability distribution of the ordering operator from the 2D/3D universal distribution is

$$\frac{1}{n}\sum_{i=1}^{n} \sqrt{y_i} \times |y_i - y_{\mathrm{Ising},i}|, \tag{5}$$

where $n$ is the total number of points of the scaling parameter $x$, $y_i$ is the probability of the $i$th point $x_i$, and $y_{\mathrm{Ising},i}$ is the Ising universal value of $x_i$. For each confined system with fixed wall separation and box size, fits of the near-critical histograms to both the 2D and 3D universal distribution were attempted, resulting in two types of apparent critical points. In the following, we call them the apparent "2D critical point" and the apparent "3D critical point" for simplicity. We use the term apparent to emphasize that the temperature and chemical potential for which the fit is optimal do not correspond to a true critical point, but rather to a poorer candidate compared with the one arising from the fit that yields the smaller deviation with respect to the corresponding universal Ising distribution. Even though one candidate is superior to the other based on the respective qualities of the fits, we locate and report both. The qualities of the fits to the 2D and 3D universal distributions were quantitatively compared using the following criterion:

$$\frac{\frac{1}{n}\sum_{i=1}^{n} \sqrt{y_i} \times |y_i - y_{\mathrm{Ising},i}|}{y_{\mathrm{Ising,peak}} - y_{\mathrm{Ising},x=0}}, \tag{6}$$

where $y_{\mathrm{Ising,peak}}$ is the peak value of the Ising universal distribution and $y_{\mathrm{Ising},x=0}$ is the "well" value of the Ising universal distribution at $x=0$. We chose the above criteria based on the following considerations: first, deviations near the peaks are assigned more weight than the deviations near the bottom by placing a weight $\sqrt{y_i}$ in the equation. We found this weight especially useful when optimizing the matches to the universality classes. Second, the deviations of the 2D and 3D matches are compared on an equivalent scale, that is, $y_{\mathrm{Ising,peak}} - y_{\mathrm{Ising},x=0}$, and thereby fall into the same range. For example, high quality matches to the 2D and 3D universality

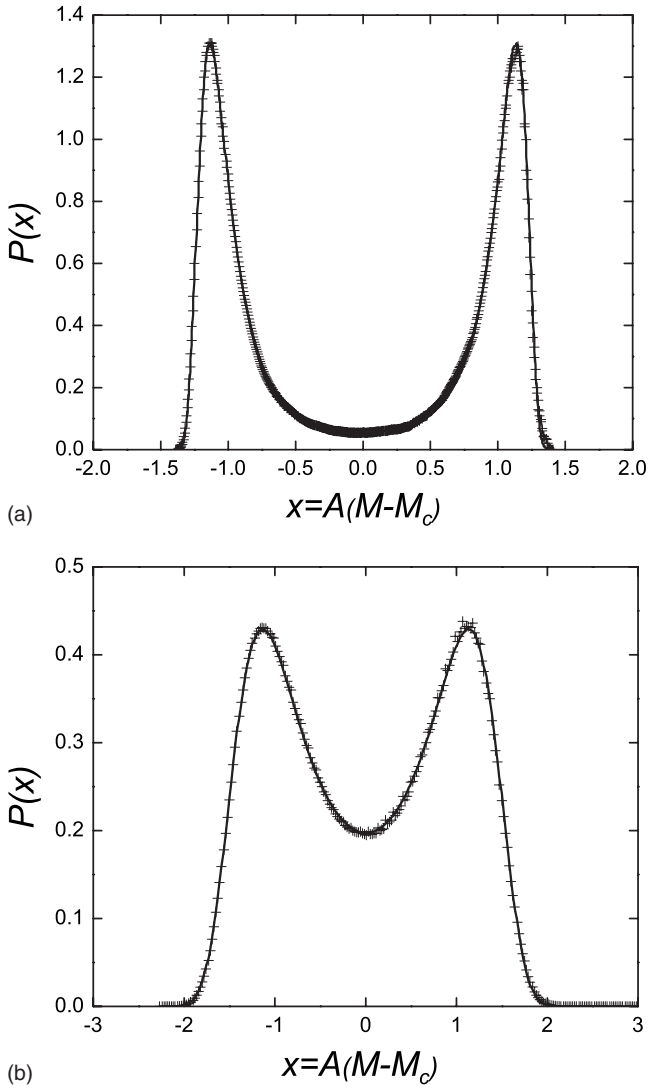


FIG. 1. Examples of fitting the probability distribution $P(x)$ for the confined Lennard-Jones fluid to the 2D and 3D universality classes, indicated by solid lines. Simulation data are indicated by +. (a) 2D fitting at $H=1$, $L_x=L_y=28$. (b) 3D fitting at $H=6$, $L_x=L_y=10$.

class (Fig. 1) yield comparable values for the deviation metric, i.e., about 0.4, whereas poor quality matches yield a deviation greater than 2.0 (see Sec. III). Using these criteria, we were able to see clearly how the system gradually approached either the 2D or 3D universality class, and observe crossovers from one to the other as the box size and wall separation change.

Finite-size scaling theory[34] predicts that the apparent critical parameters, $T_c(L)$ and $\rho_c(L)$, deviate from their infinite-system values $T_c(\infty)$ and $\rho_c(\infty)$ according to the following scaling relationships:

$$T_c(L) - T_c(\infty) \propto L^{-(\theta+1)/\nu}, \tag{7}$$

$$\rho_c(L) - \rho_c(\infty) \propto L^{-(1-\alpha)/\nu}, \tag{8}$$

where $\theta$ is the correction-to-scaling exponent, $\nu$ is the correlation length exponent, and $\alpha$ is the exponent associated with the heat capacity divergence. The values of $(\theta, \nu, \alpha)$ for the 3D and 2D Ising universality classes are (0.54, 0.63, 0.11) (Refs. 73 and 74) and (2, 1, 0),[72,75,76] respectively. By scaling the apparent 2D and 3D critical points with their corresponding exponents, the 2D and 3D critical parameters for infinite system size were obtained.

The histogram data can also be used to calculate the phase coexistence curve. This is achieved by matching the area under the vapor and liquid portion of the density probability distribution. To obtain the phase coexistence curve far below the critical point, several additional runs on both the liquid and vapor sides were conducted to cover broader ranges of densities. The additional runs on the vapor side started with an empty box, but the additional runs on the liquid side started from selected final high-density configurations from previous runs near the critical point in order to avoid hysteresis.[32]

## III. RESULTS AND DISCUSSION

Table I summarizes the critical parameters for confined LJ systems for various wall separations and box sizes. Both the apparent 2D and 3D critical points are listed, along with their deviations from the universality distributions calculated from Eq. (6). From the deviation column, it can be seen that at $H=1$, 1.2, and 1.5, the vapor-liquid transition falls into the 2D Ising universality class for all box sizes studied, with equivalently small deviations. In these systems, only one layer of particles can be accommodated in the confined region. One example of our matches to the 2D universality class for $H=1$, $L_x=L_y=28$ is shown in Fig. 1(a). The attempted matches to the 3D universality class, on the other hand, result in quite large deviations. As the wall separation increases, the quality of the fits to the two universality classes is affected by both wall separation and box size. In general, the probability distribution approaches the 2D universality class at large box sizes and small wall separations, and the 3D universality class at small box sizes and large wall separations. These trends are shown graphically in Fig. 2, where the deviations from the 2D and 3D universality classes listed in Table I are represented on a color scale (blue=0.4; red=2.8). At the largest wall separation $H=6$, and the smallest box sizes $L_x=L_y=10$ studied, the probability distribution matches the 3D universality class very well, see Fig. 1(b). The same quality of fits is also observed for $H=6$, $L_x=L_y=14$, and $H=4$, $L_x=L_y=10$. At these conditions, the probability distributions do not match the 2D universality class well due to the finite size of the system.

By comparing the deviations at each wall separation and box size, we classify the systems into four categories: (1) 2D: deviation from the 2D universality class $\leq 0.5$; (2) quasi-2D: deviation from the 2D universality class $> 0.5$, but smaller than the deviation from the 3D universality class; (3) quasi-3D: deviation from the 3D universality class $> 0.5$, but smaller than the deviation from the 2D universality class; and (4) 3D: deviation from the 3D universality $\leq 0.5$. The result is shown in Fig. 3. In this figure, we see clearly a crossover from 3D to 2D universality class, characterized by a "transition line" with a negative slope. The location of the transition line depends on the criteria and the model system used, but its existence indicates the significant impact of finite size on the determination of the effective dimensionality

TABLE I. Vapor-liquid critical parameters of confined LJ systems. (The error corresponding to the last digit is shown in parentheses.)

| | | 2D | | | | 3D | | | |
|---|---|---|---|---|---|---|---|---|---|
| H ($\sigma$) | Box size ($\sigma$) | $T_c^*$ | $\mu_c^*$ | $\rho_c^*$ | Dev.[a] | $T_c^*$ | $\mu_c^*$ | $\rho_c^*$ | Dev.[a] |
| 1 | 14 | 0.4803(10) | −1.6616(6) | 0.372(2) | 0.4(1) | 0.5072(11) | −1.6322(9) | 0.354(5) | 2.2(1) |
| | 18 | 0.4808(2) | −1.6612(7) | 0.371(4) | 0.5(2) | 0.5022(7) | −1.6372(9) | 0.360(4) | 2.2(6) |
| | 22 | 0.4810(3) | −1.6606(2) | 0.371(2) | 0.4(3) | 0.4977(7) | −1.6414(7) | 0.367(4) | 2.2(4) |
| | 28 | 0.4814(3) | −1.6604(1) | 0.371(3) | 0.4(3) | 0.4949(4) | −1.6449(4) | 0.364(4) | 2.2(7) |
| | ∞ | **0.4814(3)** | | **0.370(2)** | | **0.4925(27)** | | **0.375(9)** | |
| 1.2 | 14 | 0.4826(6) | −1.7516(14) | 0.311(1) | 0.5(2) | 0.5098(23) | −1.7266(10) | 0.298(4) | 2.1(3) |
| | 18 | 0.4830(19) | −1.7520(17) | 0.310(2) | 0.5(2) | 0.5042(23) | −1.7322(15) | 0.301(5) | 2.6(2) |
| | 22 | 0.4836(9) | −1.7514(2) | 0.310(2) | 0.5(2) | 0.5014(16) | −1.7347(14) | 0.300(9) | 2.8(15) |
| | 28 | 0.4838(8) | −1.7511(11) | 0.310(1) | 0.4(2) | 0.4995(41) | −1.7361(39) | 0.305(2) | 2.2(10) |
| | ∞ | **0.4839(3)** | | **0.309(2)** | | **0.4971(2)** | | **0.306(5)** | |
| 1.5 | 14 | 0.4934(4) | −1.8816(6) | 0.257(1) | 0.5(1) | 0.5217(7) | −1.8623(3) | 0.248(1) | 2.1(4) |
| | 18 | 0.4944(2) | −1.8810(7) | 0.256(1) | 0.4(1) | 0.5164(7) | −1.8658(11) | 0.249(1) | 2.3(2) |
| | 22 | 0.4938(12) | −1.8814(12) | 0.255(2) | 0.5(3) | 0.5118(14) | −1.8688(10) | 0.250(5) | 2.3(3) |
| | 28 | 0.4940(4) | −1.8811(12) | 0.256(1) | 0.4(1) | 0.5080(12) | −1.8712(10) | 0.252(2) | 2.8(10) |
| | ∞ | **0.4942(9)** | | **0.254(4)** | | **0.5058(39)** | | **0.254(3)** | |
| 1.8 | 14 | 0.5336(5) | −2.0423(4) | 0.241(1) | 0.9(1) | 0.5610(11) | −2.0253(4) | 0.232(2) | 1.6(4) |
| | 18 | 0.5340(6) | −2.0422(10) | 0.240(1) | 0.7(1) | 0.5552(19) | −2.0287(19) | 0.235(4) | 2.2(11) |
| | 22 | 0.5344(2) | −2.0418(8) | 0.241(1) | 0.6(1) | 0.5521(26) | −2.0306(8) | 0.232(1) | 2.0(10) |
| | 28 | 0.5346(8) | −2.0418(2) | 0.240(1) | 0.5(2) | 0.5477(15) | −2.0334(2) | 0.235(5) | 2.3(9) |
| | ∞ | **0.5347(2)** | | **0.240(1)** | | **0.5460(35)** | | **0.236(3)** | |
| 1.9 | 14 | 0.5848(14) | −2.1374(26) | 0.275(5) | 1.7(2) | 0.6075(10) | −2.1132(22) | 0.257(4) | 0.8(4) |
| | 18 | 0.5871(18) | −2.1348(34) | 0.274(4) | 1.5(2) | 0.6038(19) | −2.1168(31) | 0.258(5) | 1.2(1) |
| | 22 | 0.5870(6) | −2.1340(6) | 0.274(4) | 1.4(4) | 0.6007(10) | −2.1193(12) | 0.266(9) | 1.6(3) |
| | 28 | 0.5881(6) | −2.1336(6) | 0.274(2) | 0.9(2) | 0.5984(5) | −2.1220(8) | 0.265(4) | 1.4(5) |
| | ∞ | **0.5882(2)** | | **0.273(2)** | | **0.5968(22)** | | **0.273(4)** | |
| 2 | 14 | 0.6566(14) | −2.2580(26) | 0.308(5) | 1.8(1) | 0.6784(10) | −2.2274(17) | 0.292(2) | 0.8(1) |
| | 18 | 0.6590(18) | −2.2545(20) | 0.305(5) | 1.5(2) | 0.6750(17) | −2.2317(12) | 0.293(9) | 1.2(8) |
| | 22 | 0.6601(15) | −2.2518(11) | 0.305(4) | 1.5(6) | 0.6729(17) | −2.2334(20) | 0.295(6) | 1.2(4) |
| | 28 | 0.6603(4) | −2.2519(4) | 0.303(5) | 1.0(6) | 0.6697(7) | −2.2384(12) | 0.296(6) | 2.4(6) |
| | ∞ | **0.6611(4)** | | **0.299(1)** | | **0.6686(31)** | | **0.298(2)** | |
| 4 | 10 | 0.9178(16) | −3.0963(13) | 0.255(2) | 2.2(1) | 0.9656(5) | −3.0745(22) | 0.246(4) | 0.4(4) |
| | 14 | 0.9262(22) | −3.0940(19) | 0.253(2) | 2.1(2) | 0.9587(30) | −3.0798(16) | 0.245(7) | 0.8(6) |
| | 18 | 0.9299(21) | −3.0916(12) | 0.250(1) | 1.8(3) | 0.9536(11) | −3.0807(12) | 0.249(4) | 1.2(3) |
| | 22 | 0.9302(15) | −3.0921(12) | 0.251(2) | 1.5(2) | 0.9503(12) | −3.0833(5) | 0.243(2) | 1.2(5) |
| | ∞ | **0.9319(3)** | | **0.246(2)** | | **0.9487(48)** | | **0.248(7)** | |
| 6 | 10 | 1.0093(31) | −3.2838(23) | 0.248(2) | 2.6(2) | 1.0564(2) | −3.2668(17) | 0.235(3) | 0.4(1) |
| | 14 | 1.0201(26) | −3.2795(3) | 0.243(1) | 2.2(2) | 1.0518(16) | −3.2679(8) | 0.236(1) | 0.4(2) |
| | 18 | 1.0263(16) | −3.2769(3) | 0.243(3) | 2.2(2) | 1.0496(2) | −3.2682(11) | 0.237(7) | 0.8(4) |
| | 22 | 1.0258(8) | −3.2772(9) | 0.241(2) | 1.9(5) | 1.0460(6) | −3.2699(7) | 0.236(6) | 0.8(5) |
| | ∞ | **1.0284(11)** | | **0.236(4)** | | **1.0459(4)** | | **0.237(2)** | |

[a]Deviation corresponding to the value of Eq. (6) multiplied by 100.

of a confined system. The negative slope of this transition line suggests that in the limit of infinite box size with any finite wall separation, the system becomes 2D in terms of its critical behavior. Note that for large wall separations, the 2D critical behavior is only expected to occur in very narrow region asymptotically close to the critical point, where the correlation length for the macroscopic system diverges and exceeds the simulation box size. This figure also shows that in order for the system to approach the 2D universal distribution, a sufficiently large box must be used, especially for large wall separations, which may require a simulation box so large as to make it computationally impractical.

Table I also shows that matches to the 3D universality class result in a higher critical temperature, a lower critical density, and a higher critical chemical potential than the corresponding 2D matches. These differences become systematically smaller as the box size increases. If we apply finite-size scaling theory, specifically Eqs. (7) and (8), and plot the apparent critical temperatures and densities with their 2D and 3D scaling exponents (see Sec. II), we can obtain the extrapolations of the apparent 2D and 3D critical points to the infinite system size limit. These results are also shown in Table I. An example of this scaling relationship for $H=2$ is shown in Fig. 4. It can be observed in both Fig. 4 and Table I that the differences between the 2D and 3D critical temperatures do not completely vanish in the $L\rightarrow\infty$ limit. Specifically, the infinite-size critical temperatures extrapolated from the apparent 3D critical points are 1%–3% higher than those extrapolated from the apparent 2D critical points. In

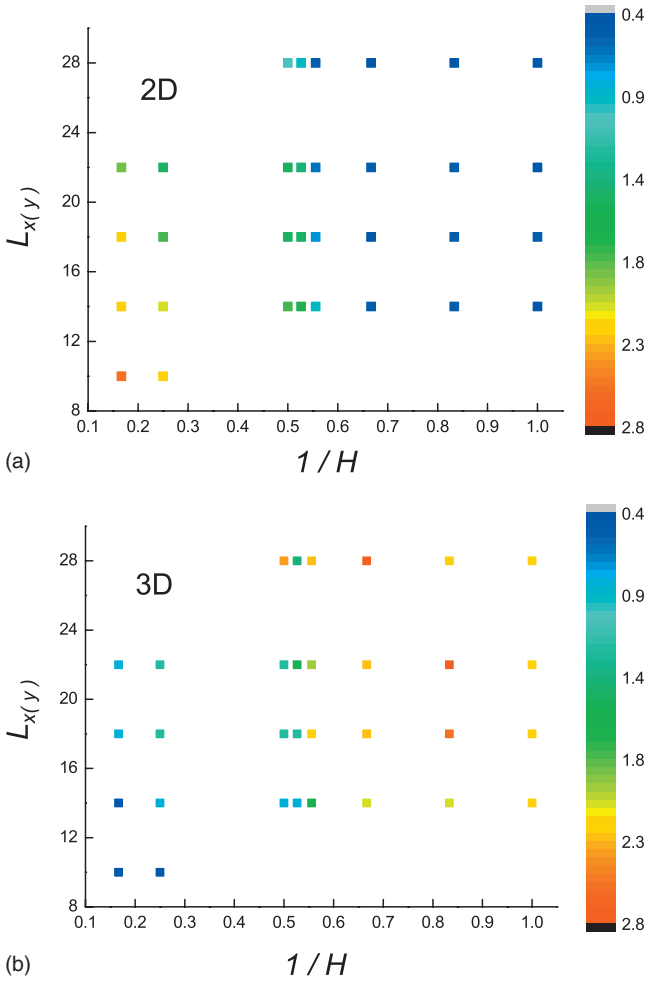


FIG. 2. Deviations from the 2D (a) and 3D (b) universal distributions as a function of system size ($L_x=L_y$) and inverse wall separation, $1/H$. Color scale runs from blue (=0.4) to red (=2.8).

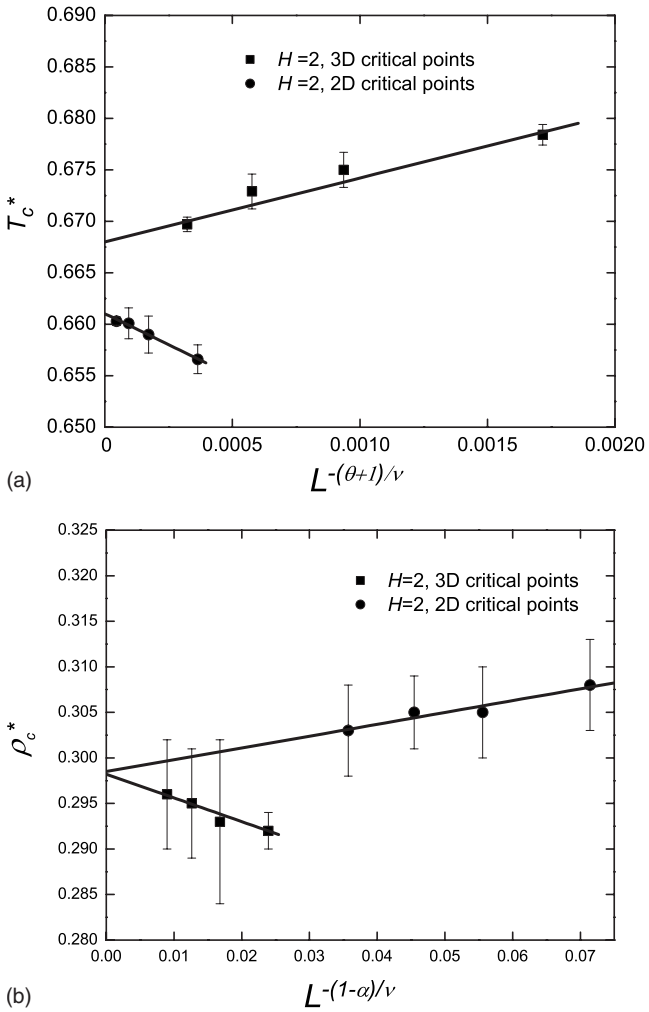


FIG. 4. Calculation of critical parameters of infinite systems by scaling the apparent critical points with 2D and 3D critical exponents at $H=2$. Confined Lennard-Jones system. (a) Critical temperature. (b) Critical density.

contrast, the 2D and 3D critical densities have differences smaller than statistical uncertainties when extrapolated to infinite system size.

Figure 5 shows the shifts of the $H$-dependent infinite-size critical temperatures obtained by applying finite-size scaling [Eq. (7)] to the apparent 2D and 3D critical points from the bulk value as a function of the inverse wall separation, $1/H$. The bulk critical parameters are from Ref. 34, which gives the following values:

$$T_c^* = 1.1876(3), \quad \rho_c^* = 0.3197(4).$$

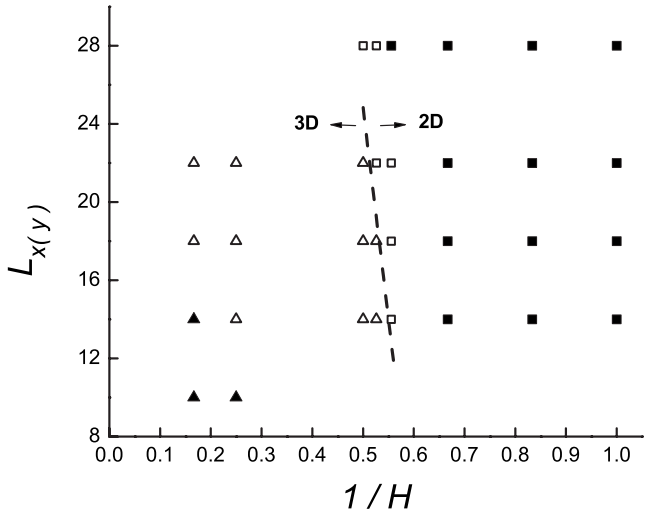


FIG. 3. Crossover from the 3D to the 2D universality class in the space of wall separation, $H$, and system size, $L_x=L_y$. Filled squares: 2D; unfilled squares: quasi-2D; unfilled triangles: quasi-3D; and filled triangles: 3D. Confined LJ system.

Consistently with previous work on confined square-well fluids,[12] the shift in the critical temperature scales linearly with $1/H$ until $H$ drops to 2, at which point the linear relationship breaks down, $T_c(H)$ undergoes a sudden jump, and then gradually approaches the strictly 2D critical point at $H=1$. Both 2D and 3D critical points are shown in the figure, and the error bars are not shown because they are smaller than the symbol size. Notice that the 2D and 3D critical points follow the same trend and their differences are minor. Figure 6 shows the behavior of the infinite-size critical density as a function of $1/H$. The data show a maximum at $H=2$, coincident with the point where the shift in the critical temperature changes abruptly, and a minimum around $H=1.8$, where the $T_c(\text{bulk})-T_c(H)$ versus $1/H$ plot undergoes a second sharp change in slope. Another minimum

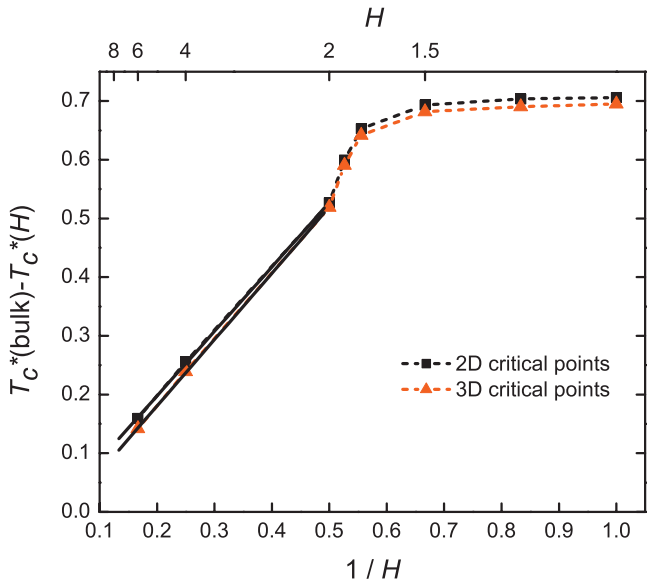


FIG. 5. Deviation of the critical temperatures from the bulk value as a function of inverse wall separation, $1/H$. Solid lines are linear fits of data for $H \geq 2$. Confined LJ system. Infinite-size critical temperatures ($L \to \infty$) were obtained by applying finite-size scaling [Eq. (7)] to the apparent 2D and 3D critical points.

should occur for $H > 6$, due to the fact that the critical parameters must approach their bulk values when $H \to \infty$.

Figure 7 shows the phase diagram determined using histogram reweighting techniques as described in Sec. II. The bulk phase diagram is from Ref. 34. The critical parameters shown in the figure are the 2D critical point parameters. The error bars are smaller than the symbol size. Unlike the critical parameters, phase coexistence densities away from the critical point are found to be unaffected by finite-size effects. It can be seen that the coexistence density of the vapor phase is only weakly affected by confinement, whereas the liquid phase is very sensitive to this physical parameter. In particular, it can be seen that the dependence of the liquid density at coexistence upon $H$ is highly nonmonotonic.

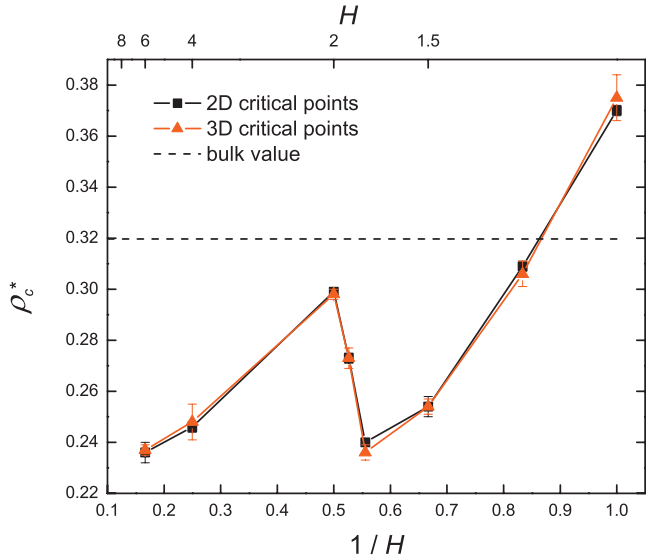


FIG. 6. Critical density as a function of wall separation. Confined LJ system. Infinite-size critical densities ($L \to \infty$) were obtained by applying finite-size scaling [Eq. (8)] to the apparent 2D and 3D critical points.

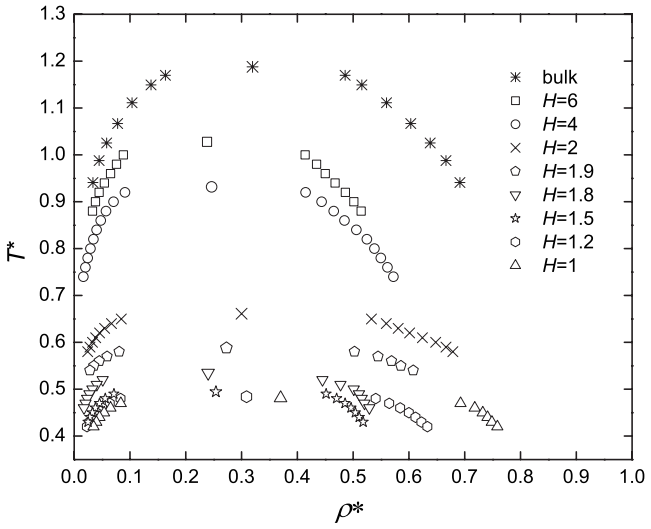


FIG. 7. Phase diagram of the confined LJ system at various wall separations.

For comparison, we show in Fig. 8 the vapor-liquid phase diagram of a more complex fluid, the rigid five-site ST2 model of water,[35] under various degrees of confinement. In this model, a water molecule has a tetrahedral structure, with an oxygen atom at the center and four point charges (two positive charges representing partially shielded protons and two negative charges) located at the vertices. The force field consists of two parts, the LJ potential between central oxygen atoms and the Coulombic interactions between charges. Characteristic parameters describing energy and size can be found in Ref. 35. To obtain the phase diagram of bulk ST2 water as well as that of ST2 water confined by hard walls, we followed the same procedure as described before for the LJ system. In bulk ST2 water, a cubic box is used. Four system sizes ($L=6\sigma$, $8\sigma$, $10\sigma$, and $12\sigma$) were studied and the infinite-system-size critical point was obtained by extrapolation. The long-range electrostatic interactions were calculated using the 3D Ewald sum. For confined ST2 water, three system sizes were used for each wall separation and the infinite-system-size critical point was obtained by extrapola-

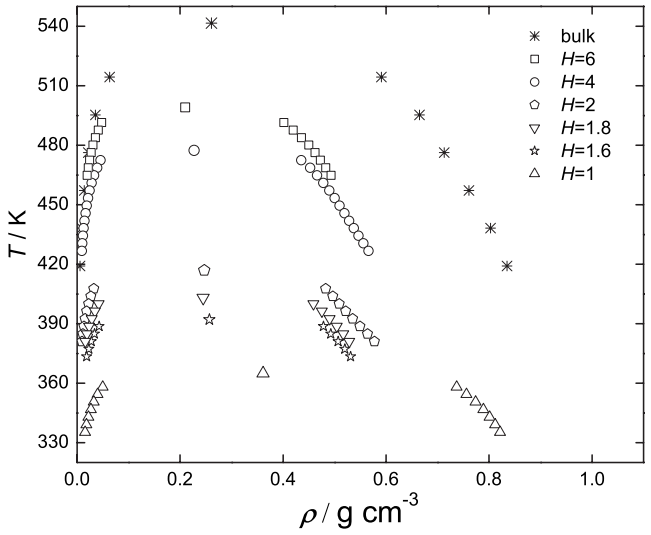


FIG. 8. Phase diagram of confined ST2 water at various wall separations.

tion. The long-range electrostatic interactions were calculated using the 3D Ewald sum with a gap in the $z$ direction between two neighbor replicas, as described in Ref. 77. The parameter describing the width of the screening charge Gaussian distribution in the Ewald sum was set to be 0.269 $Å^{-1}$. It can be seen that the main features of Fig. 7, such as the critical density maximum around $H=2$, the critical density minimum around $H=1.8$, the dependence of the coexistence densities of the vapor and liquid phases upon the extent of confinement, and the shift in the critical temperatures with $H$, are also preserved in confined ST2 water.

## IV. CONCLUSIONS

Using LJ fluids confined between parallel hard walls as a model system, we have explored the application of the mixed-field finite-size scaling method of Wilding[33,34] for determining critical parameters of phase transitions in confinement. We find that the probability distribution of the ordering operator, $P(M)$, undergoes a crossover from the 3D to the 2D Ising universality class at small enough wall separations ($H$) and large enough system sizes ($L_x=L_y\equiv L$). We define quantitative criteria for 3D, quasi-3D, quasi-2D, and 2D behavior based on matches of $P(M)$ to the 2D and 3D universal distributions. This allowed us to construct a "phase diagram" in the ($L$-$H$) plane showing the boundary between the various types of behavior.

We have shown the capability of the mixed-field finite-size scaling method in providing good estimates of the critical parameters of confined fluids using modest system sizes. We found that the infinite-size critical parameters extrapolated from the apparent 2D and 3D critical points have only minor differences.

We investigated the shifts of the critical temperature and density, and of the coexistence densities in the slitlike pores as a function of wall separation over the range $\sigma\leq H\leq 6\sigma$. Our results support the recent study of Jana *et al.*[12] in that we found at least three sharply different regions as a function of wall separation $H$:

(1) $\sigma\leq H\leq 1.8\sigma$. The critical temperature increases slowly with $H$, but the critical density drops significantly, as does the saturated liquid density.
(2) $1.8\sigma\leq H\leq 2\sigma$. The critical temperature increases sharply with $H$, the critical density increases with $H$, as does the saturated liquid density.
(3) $2\sigma\leq H\leq 6\sigma$. The shift in the critical temperature with respect to the bulk value scales linearly with the inverse wall separation, $1/H$. The critical density decreases gradually with $H$, but not the saturated liquid density.

The same behavior is also found in the phase diagram of ST2 water confined by hard slitlike walls. A fourth region very near the 3D critical point may also exist, in which the critical density should increase again to approach the 3D value.

Studies for $H>6$ and $L>28$ are beyond the scope of this work, and the extension of the crossover line in Fig. 3 to the upper left region, as well as the dependence of the critical point and coexistence densities upon $H$ for $H>6$ deserve further investigation. In addition, further work is also needed on the dependence of the 2D-3D crossover line on additional variables, such as fluid-fluid and fluid-wall interactions.

## ACKNOWLEDGMENTS

PGD gratefully acknowledges the support of the National Science Foundation (Collaborative Research in Chemistry Grant No. CHE 0404699) and BP Amoco (Carbon Mitigation Initiative at Princeton University). Additional support has been provided by the Princeton Center for Complex Materials (PCCM), a National Science Foundation funded Materials Research Science and Engineering Center, Award No. DMR-0819860. We would like to thank Professor Wilding for identifying the source of the numerical 2D Ising universal distribution.

## APPENDIX: ANALYTICAL EXPRESSION FOR THE 2-DIMENSIONAL UNIVERSAL DISTRIBUTION

In order to facilitate future studies, we present an analytical approximate expression for the 2D Ising universal order parameter distribution. The raw data of this distribution were obtained by MC simulations in Ref. 65. We use the expression

$$P(x)=\exp[-(ax^{16}+bx^2+c|x|+d)], \tag{A1}$$

with the parameters: $a=0.058137$, $b=-2.68949$, $c=-0.11235$, and $d=2.884162$, which are determined by minimizing the mean square error of Eq. (A1) from the simulation results.[65]

The above equation is motivated by the knowledge that for $x\gg 1$

$$P(x)\propto\exp(-Ax^{\delta+1}), \tag{A2}$$

and for $x\ll 1$

$$P(x)\propto\exp(-A_0-A_2x^2-A_4x^4-\cdots), \tag{A3}$$

(see Ref. 63), where the exponent $\delta$ takes the value 15 for 2D Ising model, and 4.8 for 3D Ising model.[63] $A$, $A_0$, $A_2$, and $A_4$

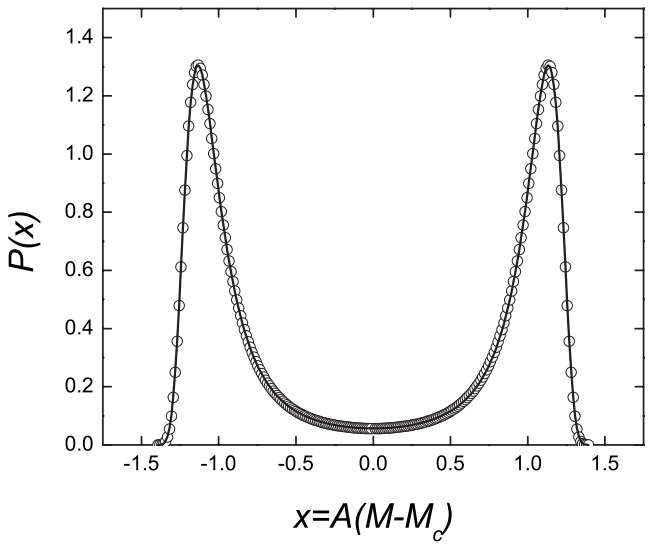


FIG. 9. 2D universality class. Circles: MC simulation data from Ref. 65. Solid line: present analytical expression [Eq. (A1)].

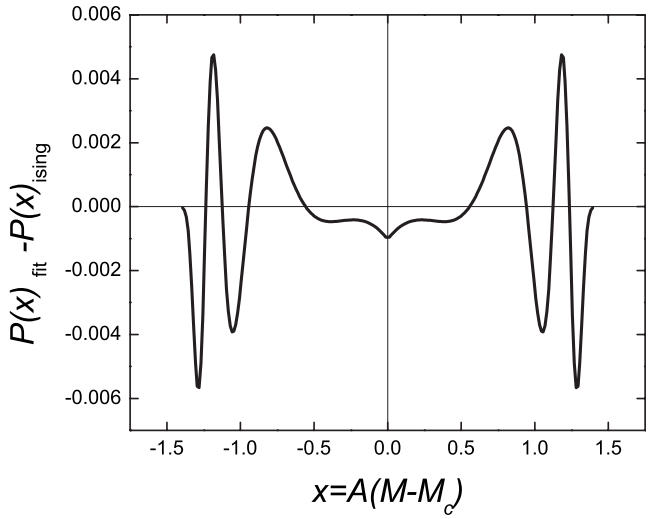


FIG. 10. Deviations of the present analytical expression, $P(x)_{\text{fit}}$, from MC simulation data of Ref. 65, $P(x)_{\text{Ising}}$.

are constants. While only even exponents, such as $x^2$, $x^4$, participate in the analytical expression of 3D Ising model by Tsypin and Blöte,[64] we found that the addition of a term $|x|$ improved the accuracy remarkably. In Fig. 9, we show the probability distribution $P(x)$ for the 2D Ising model calculated from our expression, compared to the results obtained by MC simulations.[65] In Fig. 10, we show the difference between the simulation results and our analytical results. From the plot, the maximum difference among all the points is less than 0.005. We conclude that the present expression possesses the precision needed for use in future numerical studies of 2D criticality.

[1] *Handbook of Biological Physics*, Structure and Dynamics of Membranes, edited by R. Lipowsky and E. Sackmann (Elsevier, Amsterdam, 1995), Vol. 1.
[2] R. Evans, J. Phys.: Condens. Matter **2**, 8989 (1990).
[3] J. L. England, D. Lucent, and V. S. Pande, J. Am. Chem. Soc. **130**, 11838 (2008).
[4] D. R. Cole, E. Mamontov, and G. Rother, *Neutron Applications in Earth, Energy and Environmental Sciences* (Springer, New York, 2009), p. 547.
[5] P. Chiquet, J. L. Daridon, D. Broseta, and S. Thibeau, Energy Convers. Manage. **48**, 736 (2007).
[6] L. D. Gelb, K. E. Gubbins, R. Radhakrishnan, and M. Sliwinska-Bartkowiak, Rep. Prog. Phys. **62**, 1573 (1999).
[7] J. P. Gao, W. D. Luedtke, and U. Landman, Phys. Rev. Lett. **79**, 705 (1997).
[8] K. S. Page and P. A. Monson, Phys. Rev. E **54**, R29 (1996).
[9] V. De Grandis, P. Gallo, and M. Rovere, Phys. Rev. E **70**, 061505 (2004).
[10] I. Brovchenko, A. Geiger, and A. Oleinikova, J. Chem. Phys. **120**, 1958 (2004).
[11] H. L. Vörtler, Collect. Czech. Chem. Commun. **73**, 518 (2008).
[12] S. Jana, J. K. Singh, and S. K. Kwak, J. Chem. Phys. **130**, 214707 (2009).
[13] S. K. Singh, A. Sinha, G. Deo, and J. K. Singh, J. Phys. Chem. C **113**, 7170 (2009).
[14] M. Sliwinska-Bartkowiak, S. L. Sowers, and K. E. Gubbins, Langmuir **13**, 1182 (1997).
[15] P. A. Gordon and E. D. Glandt, J. Chem. Phys. **105**, 4257 (1996).
[16] O. Sierra and Y. Duda, Phys. Lett. A **280**, 146 (2001).
[17] R. Bergman and J. Swenson, Nature (London) **403**, 283 (2000).
[18] B. Webber and J. Dore, J. Phys.: Condens. Matter **16**, S5449 (2004).
[19] A. Faraone, L. Liu, C. Y. Mou, C. W. Yen, and S. H. Chen, J. Chem. Phys. **121**, 10843 (2004).
[20] L. Liu, S. H. Chen, A. Faraone, C. W. Yen, and C. Y. Mou, Phys. Rev. Lett. **95**, 117802 (2005).
[21] F. Mallamace, M. Broccio, C. Corsaro, A. Faraone, L. Liu, C. Y. Mou, and S. H. Chen, J. Phys.: Condens. Matter **18**, S2285 (2006).
[22] S. H. Chen, F. Mallamace, C. Y. Mou, M. Broccio, C. Corsaro, A. Faraone, and L. Liu, Proc. Natl. Acad. Sci. U.S.A. **103**, 12974 (2006).
[23] F. Mallamace, M. Broccio, C. Corsaro, A. Faraone, U. Wanderlingh, L. Liu, C. Y. Mou, and S. H. Chen, J. Chem. Phys. **124**, 161102 (2006).
[24] F. Mallamace, M. Broccio, C. Corsaro, A. Faraone, D. Majolino, V. Venuti, L. Liu, C. Y. Mou, and S. H. Chen, Proc. Natl. Acad. Sci. U.S.A. **104**, 424 (2007).
[25] D. Z. Liu, Y. Zhang, C. C. Chen, C. Y. Mou, P. H. Poole, and S. H. Chen, Proc. Natl. Acad. Sci. U.S.A. **104**, 9570 (2007).
[26] F. Mallamace, C. Corsaro, M. Broccio, C. Branca, N. Gonzalez-Segredo, J. Spooren, S. H. Chen, and H. E. Stanley, Proc. Natl. Acad. Sci. U.S.A. **105**, 12725 (2008).
[27] F. Mallamace, C. Branca, M. Broccio, C. Corsaro, N. Gonzalez-Segredo, J. Spooren, H. E. Stanley, and S. H. Chen, Eur. Phys. J. Spec. Top. **161**, 19 (2008).
[28] P. H. Poole, F. Sciortino, U. Essmann, and H. E. Stanley, Nature (London) **360**, 324 (1992).
[29] J. Swenson, Phys. Rev. Lett. **97**, 189801 (2006).
[30] S. H. Chen, L. Liu, and A. Faraone, Phys. Rev. Lett. **97**, 189803 (2006).
[31] A. M. Ferrenberg and R. H. Swendsen, Phys. Rev. Lett. **63**, 1195 (1989).
[32] A. Z. Panagiotopoulos, J. Phys.: Condens. Matter **12**, R25 (2000).
[33] N. B. Wilding and A. D. Bruce, J. Phys.: Condens. Matter **4**, 3087 (1992).
[34] N. B. Wilding, Phys. Rev. E **52**, 602 (1995).
[35] F. H. Stillinger and A. Rahman, J. Chem. Phys. **60**, 1545 (1974).
[36] Y. Liu, A. Z. Panagiotopoulos, and P. G. Debenedetti, J. Chem. Phys. **131**, 104508 (2009).
[37] A. D. Bruce and N. B. Wilding, Phys. Rev. Lett. **68**, 193 (1992).
[38] K. Binder, Thin Solid Films **20**, 367 (1974).
[39] M. E. Fisher and H. Nakanishi, J. Chem. Phys. **75**, 5857 (1981).
[40] K. Binder, D. P. Landau, and M. Muller, J. Stat. Phys. **110**, 1411 (2003).
[41] F. Freire, D. Oconnor, and C. R. Stephens, J. Stat. Phys. **74**, 219 (1994).
[42] T. W. Capehart and M. E. Fisher, Phys. Rev. B **13**, 5021 (1976).
[43] O. Dillmann, W. Janke, M. Muller, and K. Binder, J. Chem. Phys. **114**, 5853 (2001).
[44] M. A. Novotny, Phys. Rev. Lett. **70**, 109 (1993).
[45] M. E. Fisher, Rev. Mod. Phys. **46**, 597 (1974).
[46] M. E. Fisher and M. N. Barber, Phys. Rev. Lett. **28**, 1516 (1972).
[47] *Finite Size Scaling and Numerical Simulation of Statistical Systems*, edited by V. Privman (World Scientific, Singapore, 1990).
[48] Y. Rouault, J. Baschnagel, and K. Binder, J. Stat. Phys. **80**, 1009 (1995).
[49] R. L. C. Vink, K. Binder, and J. Horbach, Phys. Rev. E **73**, 056118 (2006).
[50] K. Binder, J. Horbach, R. Vink, and A. De Virgiliis, Soft Matter **4**, 1555 (2008).
[51] I. Brovchenko, A. Geiger, and A. Oleinikova, J. Phys.: Condens. Matter **16**, S5345 (2004).
[52] A. R. Honerkampsmith, P. Cicuta, M. D. Collins, S. L. Veatch, M. den Nijs, M. Schick, and S. L. Keller, Biophys. J. **95**, 236 (2008).
[53] S. Jiang and K. E. Gubbins, Mol. Phys. **86**, 599 (1995).
[54] O. J. Hehmeyer, G. Arya, and A. Z. Panagiotopoulos, J. Phys. Chem. B **108**, 6809 (2004).
[55] P. G. De Gennes, J. Phys. Chem. **88**, 6469 (1984).
[56] R. L. C. Vink, Soft Matter **5**, 4388 (2009).
[57] M. P. Allen and D. J. Tildesley, *Computer Simulation of Liquids* (Clarendon, Oxford, 1987).
[58] M. E. van Leeuwen and B. Smit, J. Phys. Chem. **99**, 1831 (1995).
[59] D. Möller and J. Fischer, Fluid Phase Equilib. **100**, 35 (1994).
[60] J. J. Potoff and A. Z. Panagiotopoulos, J. Chem. Phys. **109**, 10914 (1998).
[61] A. Z. Panagiotopoulos, Int. J. Thermophys **15**, 1057 (1994).
[62] A. Vishnyakov, E. M. Piotrovskaya, E. N. Brodskaya, E. V. Votyakov, and Y. K. Tovbin, Langmuir **17**, 4451 (2001).
[63] R. Hilfer and N. B. Wilding, J. Phys. A **28**, L281 (1995).
[64] M. M. Tsypin and H. W. J. Blöte, Phys. Rev. E **62**, 73 (2000).
[65] D. Nicolaides and A. D. Bruce, J. Phys. A **21**, 233 (1988).
[66] B. Smit, J. Chem. Phys. **96**, 8639 (1992).
[67] J. Mittal, J. R. Errington, and T. M. Truskett, J. Chem. Phys. **126**, 244708 (2007).
[68] D. Frenkel and B. Smit, *Understanding Molecular Simulation: From Algorithms to Applications*, 2nd ed. (Academic, New York, 2002).

[69] M. Martin-Betancourt, J. M. Romero-Enrique, and L. F. Rull, Mol. Phys. **107**, 563 (2009).
[70] A. Z. Panagiotopoulos, V. Wong, and M. A. Floriano, Macromolecules **31**, 912 (1998).
[71] C. W. Hsu, J. Largo, F. Sciortino, and F. W. Starr, Proc. Natl. Acad. Sci. U.S.A. **105**, 13711 (2008).
[72] P. H. L. Martins and J. A. Plascak, Phys. Rev. E **76**, 012102 (2007).
[73] J. V. Sengers and J. M. H. L. Sengers, Annu. Rev. Phys. Chem. **37**, 189 (1986).
[74] A. J. Liu and M. E. Fisher, Physica A **156**, 35 (1989).
[75] J. M. Yeomans, *Statistical Mechanics of Phase Transitions* (Clarendon, Oxford, 1992).
[76] J. Salas and A. D. Sokal, J. Stat. Phys. **98**, 551 (2000).
[77] I. C. Yeh and M. L. Berkowitz, J. Chem. Phys. **111**, 3155 (1999).